On the Descriptive Geometric Interpretation of Pauli Principle, Elements of the Mendeleev Table of Chemical Elements, and the Newtonian Laminar Current of a Liquid

Alexander V. Yurkin
Puschino, Russia. E-mail: alvl1yurkin@rambler.ru

This work presents a two-dimensional and three-dimensional geometrical research of a ray system. We consider trajectories of motion of the particles having a half-integer spin. Interpretation of Pauli Principle showing distribution of electrons on power levels of the atom is given herein. The number of the electron shells in our model of the atom doesn't exceed 8. We give a geometric interpretation of the main, azimuthally, magnetic and spin numbers in the form of angles and distances. We show forth that the hyperbolic dependence of energy on the main quantum number n of the hydrogen atom ($E_n \sim -1/n^2$) known from experimental spectral studies, Bohr's theory and Quantum Mechanics can also be obtained from our geometrical formulation of Pauli Principle. Also, in the framework of research of the suggested ray model, the step structure of the layers at a laminar current of a liquid is deduced.

Contents

Introduction 149
1. Half-integer system of eight groups of rays 150
1.1. Two-dimensional projection of Gaussian (paraxial) rays 150
1.2. Three-dimensional projection of Gaussian (paraxial) rays 150
1.3. Periodic and acyclic trajectories 150
1.4. Periodic trajectories and step layers in the laminar current of a liquid 152
2. Gaussian (paraxial) rays and Pauli Principle 159
2.1. Angles, distances and quantum system 159
2.2. Periodic tables and geometrical constructions 160
2.2.1. Creation of the first shell of a quantum system 160
2.2.2. Creation of the second shell of a quantum system 160
2.2.3. Creation of the third and fourth shells of a quantum system 160
2.2.4. Pauli Principle and the geometric system of the hydrogen atom 162
Conclusions 167
Acknowledgements 167
References 167
Appendix 168

Introduction

Descriptive geometric models are used for the evident description of various phenomena, including quantum phenomena [1].

In works [2, 3], we already introduced a geometric model on the plane consisting of systems of paraxial rays describing distribution of light in lasers, turbulent and laminar flows of a liquid on pipes, and also finding an electron in the infinite deep potential. In work [3] we noted that the aforementioned model can be used for a descriptive interpretation of moving particles with the integer or half-integer spin.

In the works [3, 4] it was devoted to study the integer ray system (see [3]) by such means that possible to describe moving particles having the integer spin. However, even in the works [2, 5] we actually investigated a systems of ray trajectories which can be characterized as a half-integer ray system [3] by means of which it is possible to describe moving particles having a half-integer spin.

We aim, in the present work, to study a half-integer ray system, two-dimensional and three-dimensional geometric models of motion of the particles having a half-integer spin.

A geometric interpretation of Pauli Principle showing distribution of electrons on energy levels of the atom (such as those described in the physics textbooks [6, 7]) is suggested herein.

The geometric interpretation of the main, azimuthally, magnetic and spin numbers is given in the present work in the form of small angles and distances.

Also, we show a possibility of the existence of the final number of electron shells in the elements of the Mendeleev Periodic System of Chemical Elements. The shells and subshells of the atoms are interpreted as a system of the wave trajectories consisting of direct inclined pieces.

Geometric interpretations of the hydrogen atom and its power levels respectively are separately given in the work as well.

So forth, on the basis of the research of the half-integer ray model, we introduce the step structure of layers in a laminar current of a liquid (such a liquid is described in most textbooks, see [8]).*

*The laminary liquid current was first described long time ago by Newton. The Netwon theory was rechecked many times (see [8]).

Numerical calculations, presented in the present work, as well as those published in [3], were represented by means of three-dimensional tables created in Excel.

For the convenience of readers, reference drawings taken physics textbooks are given in Appendix, while the research part of our publication contains only originally calculated drawings and tables.

1 Half-integer system of eight groups of rays

1.1 Two-dimensional projection of Gaussian (paraxial) rays

In the work [3], we briefly described a paraxial binary (sharing in two) flat system of trajectories. This system consists of groups of rays, in which the rays are inclined under p angles, small to an axis, multiple to the angle γ:

$$p = \left(i + \frac{1}{2}\right)\gamma, \qquad i = 0, \pm1, \pm2, \ldots \tag{1}$$

We called this system of rays: "$(i + 1/2)\gamma$-system" or *half-integer ray system* [3]. We will describe this system in more detail in Fig. 1.

This binary system of rays consists of eight groups of the rays and their links. The rays and links of each of these groups aren't imposed on the rays of other groups, but can cross them.

Branching points of the rays will be spaced from a symmetry axis on small distances of q, multiple to $\frac{1}{2}k$ length:

$$q = \frac{jk}{2}, \qquad j = 0, \pm1, \pm2, \ldots \tag{2}$$

Further, we more precisely will refer to "$(i + 1/2)\gamma$-system" as "$[\, p = (i + 1/2)\gamma,\ q = jk/2\,]$-system".

In this work, as well as in the previous works [2–5] we assume that the rays extend along the branching links; therefore the number of the rays $\mathbb{N}$ can be summarized. We also assume that $\mathbb{K}$ is a number of the links generally $\mathbb{N} \geqslant \mathbb{K}$.

In Fig. 1 (a-d, f-i) eight groups of rays of the aforementioned $[\, p = (i + 1/2)\gamma,\ q = jk/2\,]$-system are shown: $\boldsymbol{K''}$, $\boldsymbol{L''}$, $\boldsymbol{M''}$, $\boldsymbol{N''}$, $\boldsymbol{O''}$, $\boldsymbol{P''}$, $\boldsymbol{Q''}$, $\boldsymbol{R''}$.

This system is placed on a rectangular *coordinate grid*. The size of a cell of a grid has height of $\frac{1}{2}k$ and length of L, $L \gg \frac{1}{2}k$, $L \gg \frac{1}{2}jk$.

Groups in Fig. 1 (a-d) and in Fig. 1 (f-i) are shifted from each other down on the $\frac{1}{2}k$ distance. Groups in Fig. 1 (f-i) are shifted concerning groups in Fig. 1 (a-d) on distance of L.

In Fig. 1 (e) and Fig. 1 (j) the image of groups of the rays $\boldsymbol{K''}$, $\boldsymbol{L''}$, $\boldsymbol{M''}$, $\boldsymbol{N''}$ and $\boldsymbol{O''}$, $\boldsymbol{P''}$, $\boldsymbol{Q''}$, $\boldsymbol{R''}$ respectively, are combined altogether. In Fig. 1 (k) all eight groups of rays are combined together.

1.2 Three-dimensional projection of Gaussian (paraxial) rays

In the work [3] we considered the three-dimensional image of a binary paraxial system of rays in the form of a nonlinear arithmetic parallelepiped: *In a nonlinear arithmetic parallelepiped all numbers are located in the rectangular planes of identical sizes, and these planes are located layer-by-layer one under another since parallelepiped top*.

In this case, the nonlinear arithmetic parallelepiped [3] has a $\mathfrak{N}L$ height, a length of $D = \frac{1}{2}km' + 1$ and a width $\Gamma = \gamma m + 1$, where L, k are distances, while γ is a small angle in the two-dimensional binary ray system (Fig. 1) and at the same time a small distance in a three-dimensional nonlinear parallelepiped [3], and $\mathfrak{N}$, m, m' are natural numbers or zero.

After a large number of passes (iterations) of $\mathfrak{N} \to \infty$ and $\mathfrak{N}L \gg L$, we write down the rule of consecutive filling with numbers of a nonlinear arithmetic parallelepiped as well as in [3]:

$$A = B + C, \tag{3}$$

where

$$A = \begin{pmatrix} \mathfrak{N} \\ p \\ q \end{pmatrix}, \quad B = \begin{pmatrix} \mathfrak{N} - 1 \\ p - 1 \\ q + p - 1 \end{pmatrix}, \quad C = \begin{pmatrix} \mathfrak{N} - 1 \\ p + 1 \\ q + p + 1 \end{pmatrix}.$$

For creation of various types [3] of nonlinear arithmetic parallelepipeds it is necessary to set various additional boundaries and initial conditions.

1.3 Periodic and acyclic trajectories

The system $[\, p = (i + 1/2)\gamma,\ q = jk/2\,]$ of rays generally consists of periodic and acyclic trajectories. In Fig. 2, one of eight groups of the rays of this system are shown for the case of $D = 4k$, $\Gamma = 7\gamma$.

We will set the *first boundary conditions* [3] for number A in formula (3) for nonzero $\mathfrak{N}$-layers:

$$A = 0 \tag{4}$$

for $q = |\, q_{max}|$, where $q_{max} = \frac{1}{2}D$.

Further we will set the *first boundary conditions* for numbers B and C in formula (3) for nonzero $\mathfrak{N}$-layers:

$$B = 0, \qquad C = 0 \tag{5}$$

for $|\, q + p - 1\,| > q_{max}$ and $|\, q + p + 1\,| > q_{max}$ rectively.

We now set the initial conditions [3] for the numbers B and C in formula (3) for the sequence of numbers q of a zero layer ($\mathfrak{N} = 0$):

$$\begin{pmatrix} 0 \\ p \\ q \end{pmatrix} = 1 \tag{6}$$

for $|q| \leqslant q_{max}$ and

$$\begin{pmatrix} 0 \\ p \\ q \end{pmatrix} = 0 \tag{7}$$

for other q.

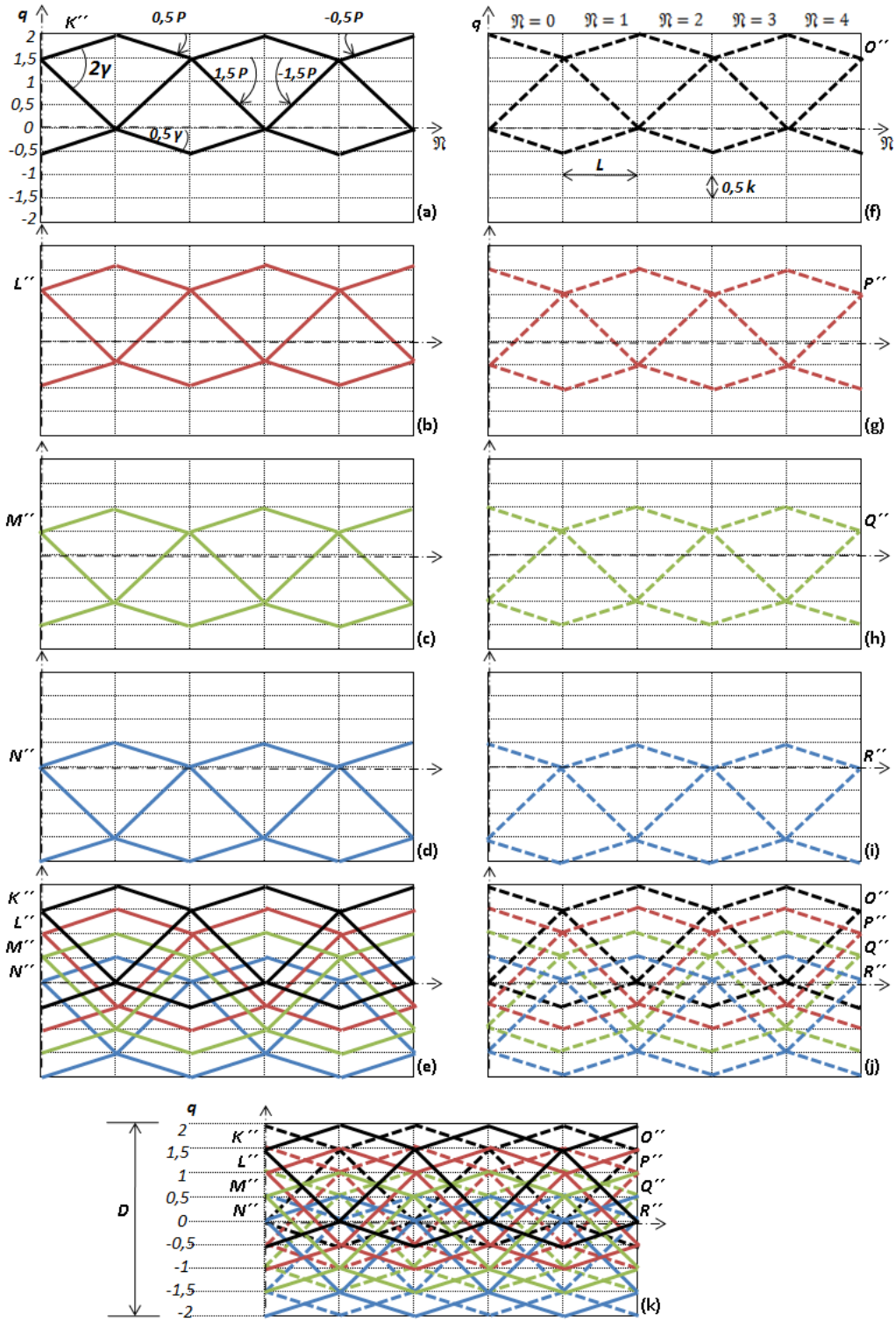

Fig. 1: Periodic trajectories. Eight groups of rays: $\boldsymbol{K''}$, $\boldsymbol{L''}$, $\boldsymbol{M''}$, $\boldsymbol{N''}$, $\boldsymbol{O''}$, $\boldsymbol{P''}$, $\boldsymbol{Q''}$, $\boldsymbol{R''}$ of the $[\, p = (i + 1/2)\,\gamma,\ q = jk/2\,]$ system. $k/2$, and L are the minimum distances on a vertical and a horizontal respectively. $\mathfrak{N}$ is the number of pass of rays (the number of iteration). Dash-dotted lines with arrows showed axes of a coordinate grid in which trajectories are placed.

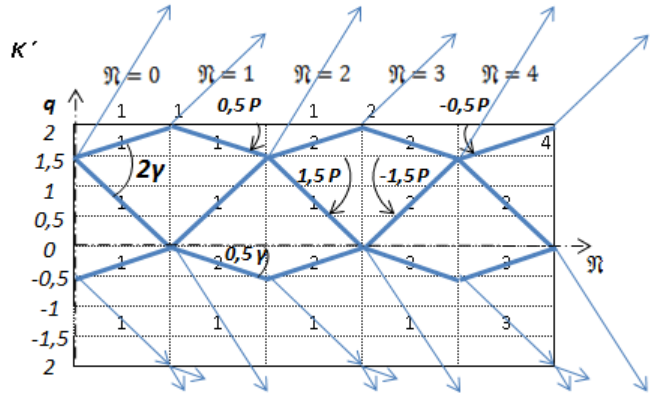

Fig. 2: Periodic and acyclic trajectories. One of eight groups of rays (K' group) of the [$p = (i + 1/2)\,\gamma,\ q = jk/2$] system is shown here. Figures about the shown links illustrate the number of the rays of $\mathbb{N}$ and the summation process of number of the rays extending along the number of the links $\mathbb{K}$ for the first five passes ($\mathfrak{R} = 0 - 4$).

In Fig. 3, calculation formulas (given in MS Excel) of a nonlinear arithmetic parallelepiped (Figs. 1, 2) for $D = 4k$, $\Gamma = 7\gamma$ case for zero, the first and second passes of the ray system, i.e. $\mathfrak{R} = 0, 1, 2$. The calculation was made according to the rule (3) of the consecutive filling with the numbers of an arithmetic rectangle taking into account the boundary (4, 5) and the initial (6, 7) conditions. Three rectangles in Fig. 3 are the layers of a nonlinear arithmetic parallelepiped.

Results of numerical calculation for the first five passes of rays, i.e. $\mathfrak{R} = 0 - 5$ are given in Fig. 4. Five rectangles are layers of a nonlinear arithmetic parallelepiped.

Results of numerical calculations for 32 pass of rays, i.e. for $\mathfrak{R} = 32$ (a) are given in Fig. 5. The envelopes of distribution of number of rays of $\mathcal{K}(q)$ on the section (b) and $\mathcal{K}'(p)$ at the angle (c) are provided.

1.4 Periodic trajectories and step layers in the laminar current of a liquid

In a specific case, the $[p = (i + 1/2)\gamma, q = jk/2]$ system of rays consists only of *periodic trajectories*. Fig. 6 shows one of the eight groups of rays of this system for the case, where $D = 4k$, $\Gamma = 3\gamma$.

In this case, we need to further set special initial and threshold conditions to create the appropriate nonlinear arithmetic parallelepiped [3].

Let's consider here a simple and illustrative (as compared to the description given in [3]) way (an Excel algorithm) of setting special initial and threshold conditions for the parallelepiped that describes the system consisting only of periodic trajectories.

Let's set the *second* threshold conditions for A, B, and C in formula (3) for nonzero $\mathfrak{R}$-layers:

$$A = 0, \tag{8}$$

if $B = 0$ and $C = 0$, and

$$B = 0 \quad \text{and} \quad C = 0, \tag{9}$$

if $A = 0$.

Let's set additional initial conditions for B and C for a zero layer ($\mathfrak{R} = 0$):

$$B = 0 \quad \text{and} \quad C = 0, \tag{10}$$

if $A = 0$.

The offered way (the algorithm) can be easily implemented in numerical calculations in Excel.

At first, we completely fill with units a numerical rectangle of the zero layer ($\mathfrak{R} = 0$) according to formula (6) and formula (7).

Then we fill with numbers a numerical rectangle of the first layer ($\mathfrak{R} = 1$) according to formulas (3 to 5). Some zeroes appear in the first layer.

Then we delete numbers (units) from the cells of the zero-layer rectangle which don't influence cells of the first-layer rectangle.

Then we delete numbers from the cells of the first-layer rectangle which don't depend on the cells of the zero-layer rectangle. We have some new zeroes in the first layer again.

Then again we delete numbers (units) from the cells of the zero-layer rectangle which don't influence the cells of the first-layer rectangle.

And so we repeat this process several times. As a result, we still have cells filled with meaningful numbers which influence other cells, and the cells which depend on other cells. The remained cells describe the $[p = (i + 1/2)\gamma, q = jk/2]$ system consisting only of periodic trajectories.

$[p = (i + 1/2)\gamma, q = jk/2]$ is the system of rays consisting only of periodic trajectories as shown in Fig. 7. The results of calculation of a nonlinear arithmetic parallelepiped (Figs. 1 and 6) are for $D = 4k$, $\Gamma = 3\gamma$ for the zero, first, and second passes of the ray system, i.e. ($\mathfrak{R} = 0, 1, 2$). The calculation was made according to the rule (3) of consecutive filling with numbers of an arithmetic rectangle taking into account the *first* and the *second* threshold (4 and 5; 8 and 9) and initial (6, 7, and 10) conditions, including the algorithm (8 to 10). The three rectangles shown in Fig. 7 are the layers of a nonlinear arithmetic parallelepiped.

Fig. 8 shows the images of layers of a nonlinear arithmetic parallelepiped and a numerical example of calculation of the $[p = (i + 1/2)\gamma,\ q = jk/2]$ system of periodic trajectories (Fig. 7) for $D = 4k$, $\Gamma = 3\gamma$ for zero and the subsequent four passes of rays, i.e. for $\mathfrak{R} = 0 - 4$.

Fig. 9 shows numerical calculations and graphics made in Excel. Numerical calculation for the 32nd pass of rays, i.e. for $\mathfrak{R} = 32$, is given in (a). It also shows the envelopes of distribution of the number of rays of $\mathcal{N}(q)$ on the section (b) and $\mathcal{N}'(p)$ at the angle (c) for $D = 4k$, $\Gamma = 3\gamma$.

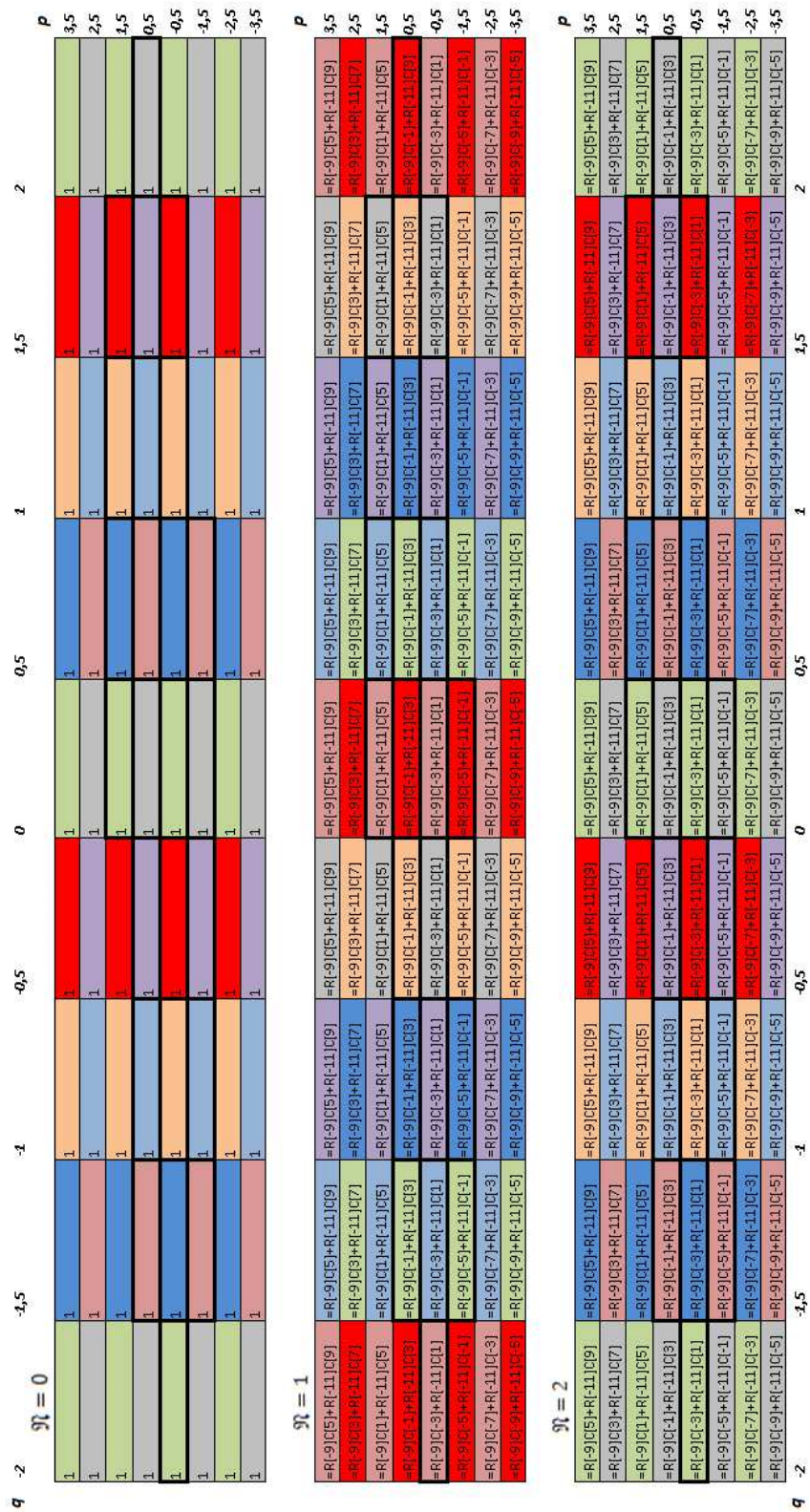

Fig. 3: Calculation of the filling with the numbers of a nonlinear arithmetic parallelepiped for $D = 4k$ case in Excel. The $[\, p = (i + 1/2)\,\gamma,\ q = jk/2\,]$ system of 8 groups of rays of periodic and acyclic trajectories; the first three pass through the rays. Each of the eight groups is marked by an own color.

Fig. 4: Results of numerical calculation in Excel for the first five passes of rays (iterations). Arrows showed dependent cells. Each of eight groups $\boldsymbol{K'}$, $\boldsymbol{L'}$, $\boldsymbol{M'}$, $\boldsymbol{N'}$, $\boldsymbol{O'}$, $\boldsymbol{P'}$, $\boldsymbol{Q'}$, $\boldsymbol{R'}$ of the $[\, p = (i + 1/2)\,\gamma,\ q = jk/2\,]$ system of periodic and acyclic trajectories. Each of the eight groups is marked by an own color.

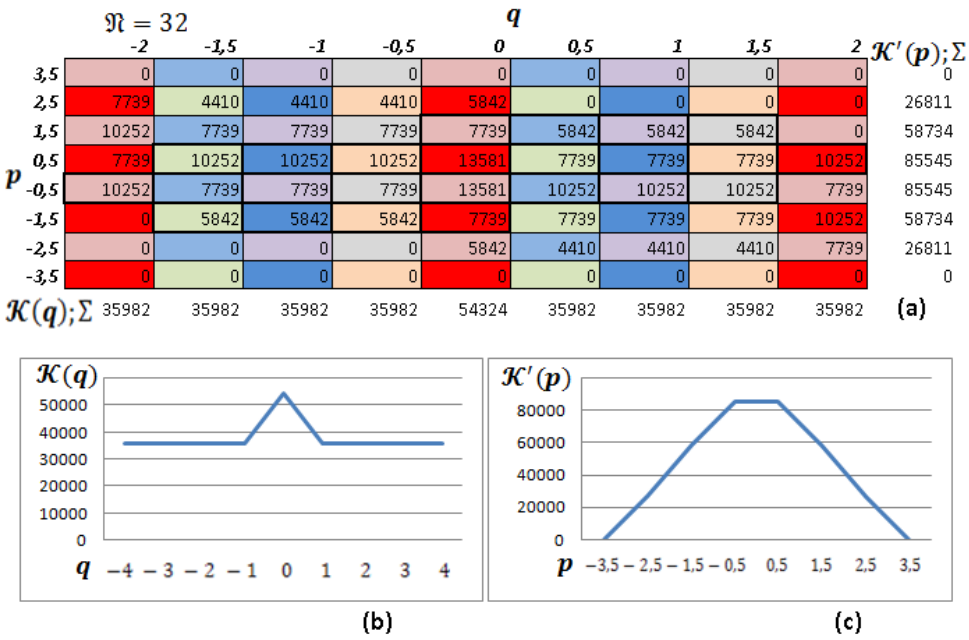

Fig. 5: Results of the numerical calculations for 32 pass of rays, i.e. for $\mathfrak{N} = 32$ for periodic and acyclic trajectories of the considered $[\,p = (i + 1/2)\,\gamma,\ q = jk/2\,]$ system (a); each of the eight groups of the system is marked by an own color; a thick framework in the central part is noted the system of periodic trajectories. The envelopes of distribution of the number of the rays of $\mathcal{K}(q)$ on the section (b) and $\mathcal{K}'(p)$ at the angle (c) are given. We note that for this case, as show our calculations, the form of envelope (b, c) practically doesn't change approximately after the 15th pass.

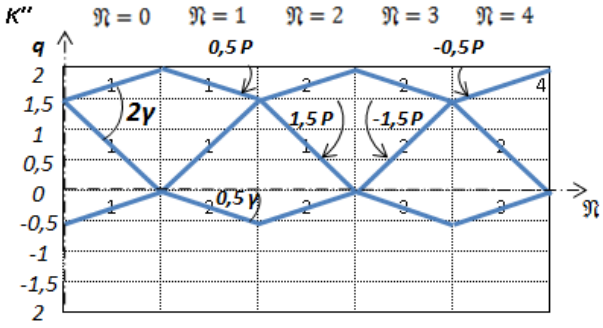

Fig. 6: Periodic trajectories. It shows one of eight groups of rays (***K″*** group) of the $[p = (i + 1/2)\gamma,\ q = jk/2]$ system.

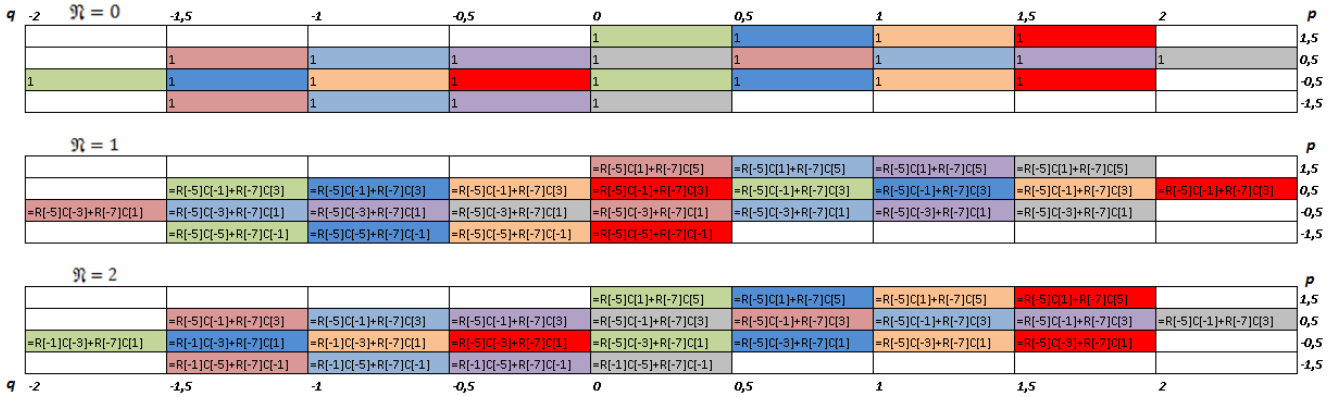

Fig. 7: Calculation of filling with numbers of a nonlinear arithmetic parallelepiped for $D = 4k$ in Excel, and the $[p = (i + 1/2)\gamma,\ q = jk/2]$ system of eight groups of rays of periodic trajectories — the first three passes of rays. Each of the eight groups is marked in a separate color.

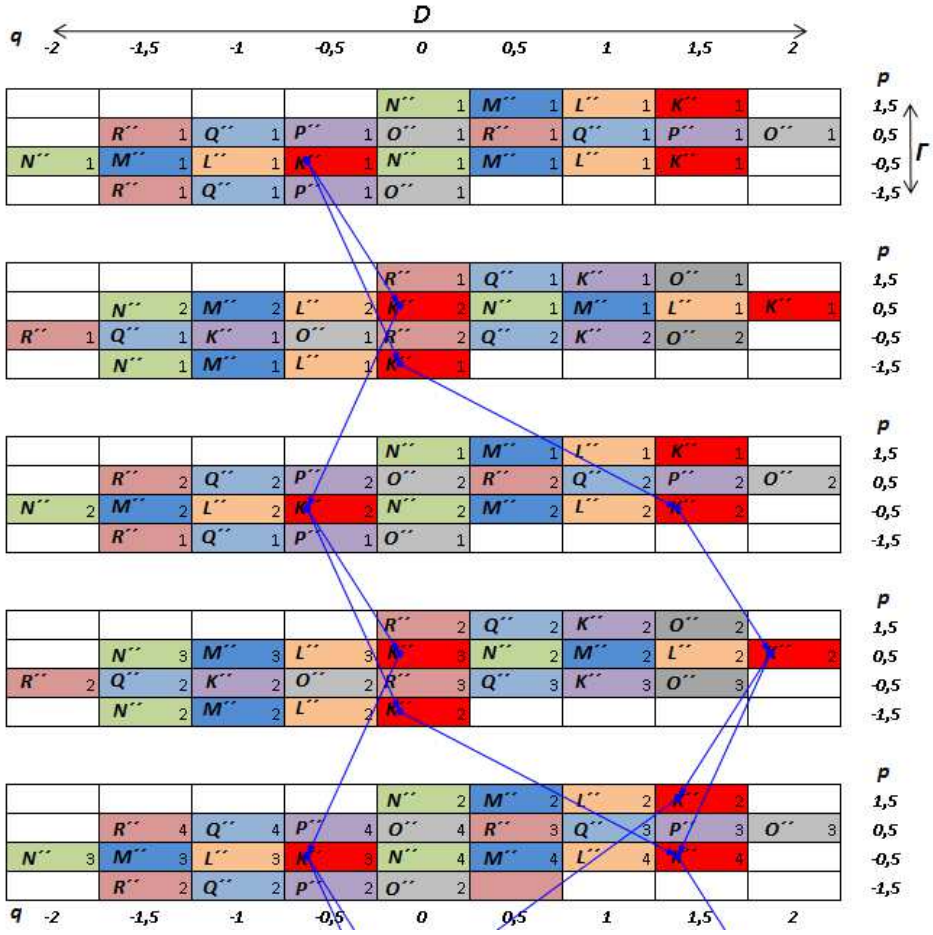

Fig. 8: Results of numerical calculation in Excel for the first five passes of rays (iterations). The arrows point to dependent cells. Each of the eight groups — $\boldsymbol{K''}$, $\boldsymbol{L''}$, $\boldsymbol{M''}$, $\boldsymbol{N''}$, $\boldsymbol{O''}$, $\boldsymbol{P''}$, $\boldsymbol{Q''}$, and $\boldsymbol{R''}$ — of the $[p=(i+1/2)\gamma,\ q=jk/2]$ system of periodic trajectories is marked in a separate color.

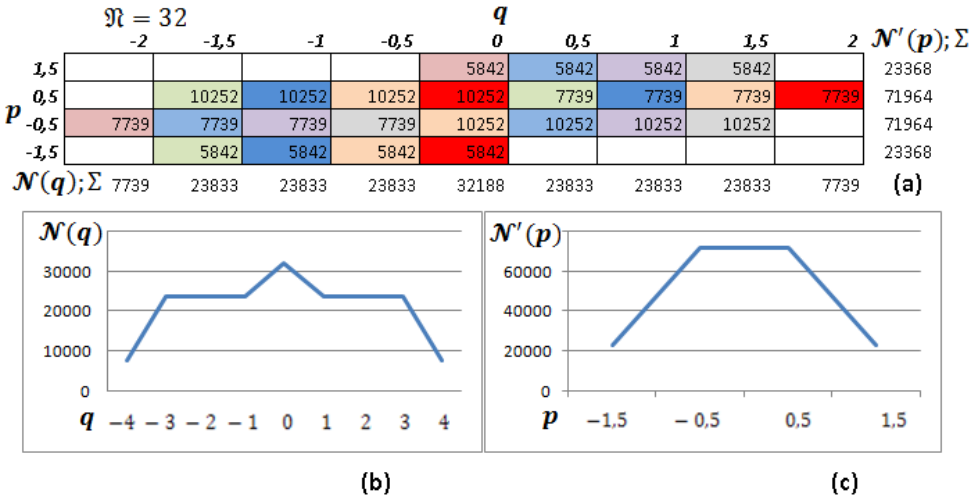

Fig. 9: Results of numerical calculations for the 32nd pass of rays, i.e. for $\Re = 32$, for periodic trajectories of the $[p=(i+1/2)\gamma,\ q=jk/2]$ system (a). Each of the eight groups of the system is marked in separate color. It also shows the envelopes of distribution of number $\mathbb{N}$ of rays of $\mathcal{N}(q)$ on the section (b) and $\mathcal{N}'(p)$ at the angle (c). Note, according to our calculations, in this case, there is virtually no change in the form of the envelope, (b) and (c), approximately after the 15th pass.

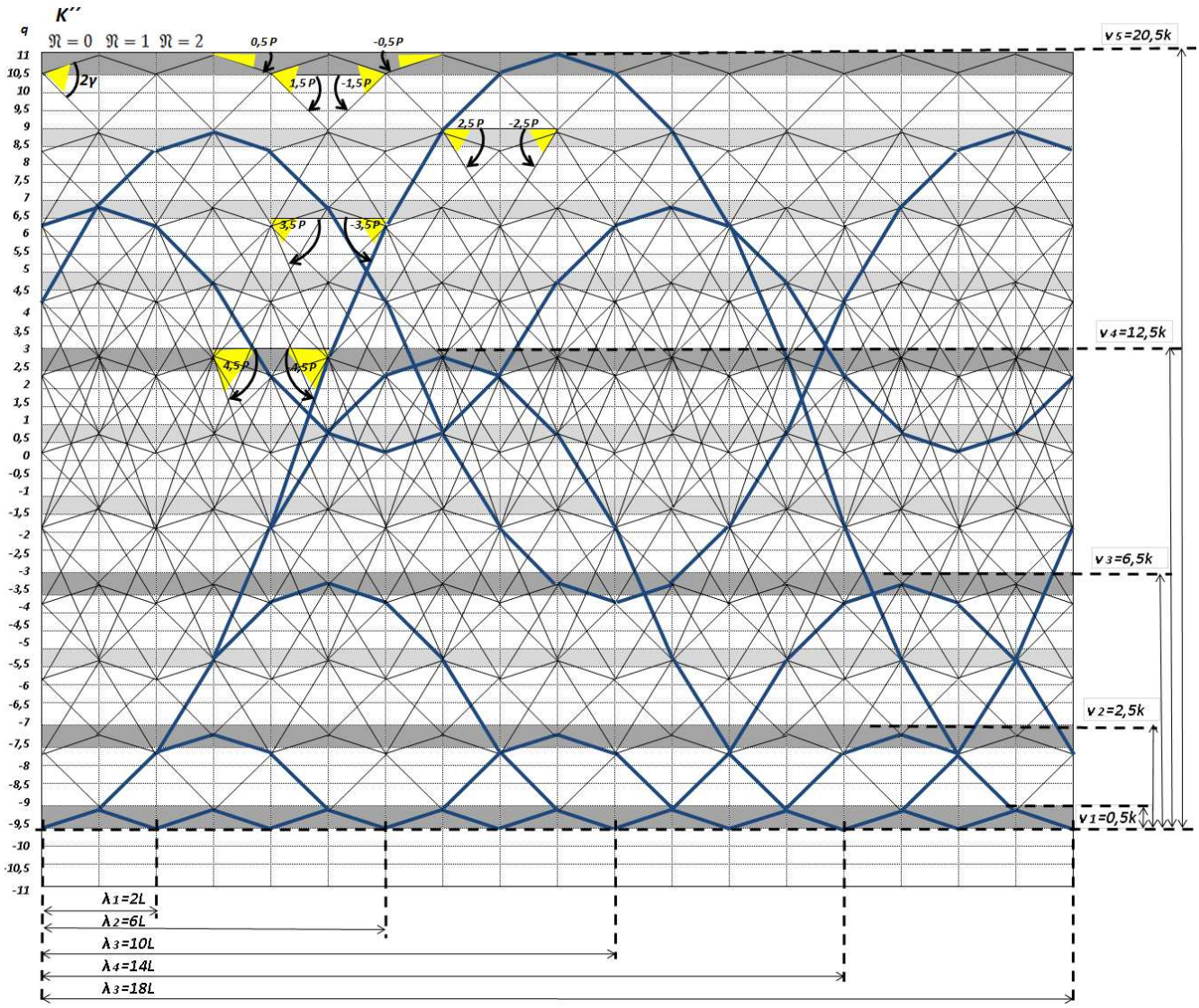

Fig. 10: Periodic (wavy) trajectories. It shows one of the eight groups of rays (***K''*** group) of the $[p=(i+1/2)\gamma,\ q=jk/2]$ system. The group contains 35 links within one pass of $\mathfrak{R}$. Crests and troughs of the "waves" are located (attached) between the horizontals marked in dark color. These horizontals have thickness of $0,5k$ and are located at identical distance of $2k$ from each other.

Fig. 10, similar to Figs. 1 and 6, shows one of the eight groups of rays of the $[p=(i+1/2)\gamma,\ q=jk/2]$ system of rays of periodic trajectories for $D=22k$, $\Gamma=9\gamma$.

In Fig. 10, some of wavy geometric trajectories for the considered $[p=(i+1/2)\gamma, q=jk/2]$ system of rays are shown as heavy lines. Wavy trajectories consist of the links inclined at small angles of $p=(i+1/2)\gamma$. The D size of the binary ray system can accommodate one "wave" or packages of "waves" of different length.

Let's denote the length of wavy trajectories by λ_n. With increasing D this λ_n is growing discretely:

$$\lambda_n = 2\,(2n-1)\,L, \tag{11}$$

where $n=1,2,\ldots$

Let's denote the height of this "wave" by ν_n. The ν_n height is proportional to the squared λ_n length:

$$\nu_n = \frac{\left(n^2-n+\frac{1}{2}\right)}{k} \sim \lambda_n^2 . \tag{12}$$

Wavy trajectories in Fig. 10 can settle down in any part of the *coordinate grid* between horizontals within D.

Fig. 11, similar to Fig. 9, shows numerical calculations and graphs made in Excel. Numerical calculation for the 128th pass of rays, i.e. for $\mathfrak{R}=128$, is given in (a). There are also envelopes of distribution of number $\mathbb{N}$ of rays of $\mathcal{N}(q)$ on the section (b) and $\mathcal{N}'(p)$ at the angle (c) given for the

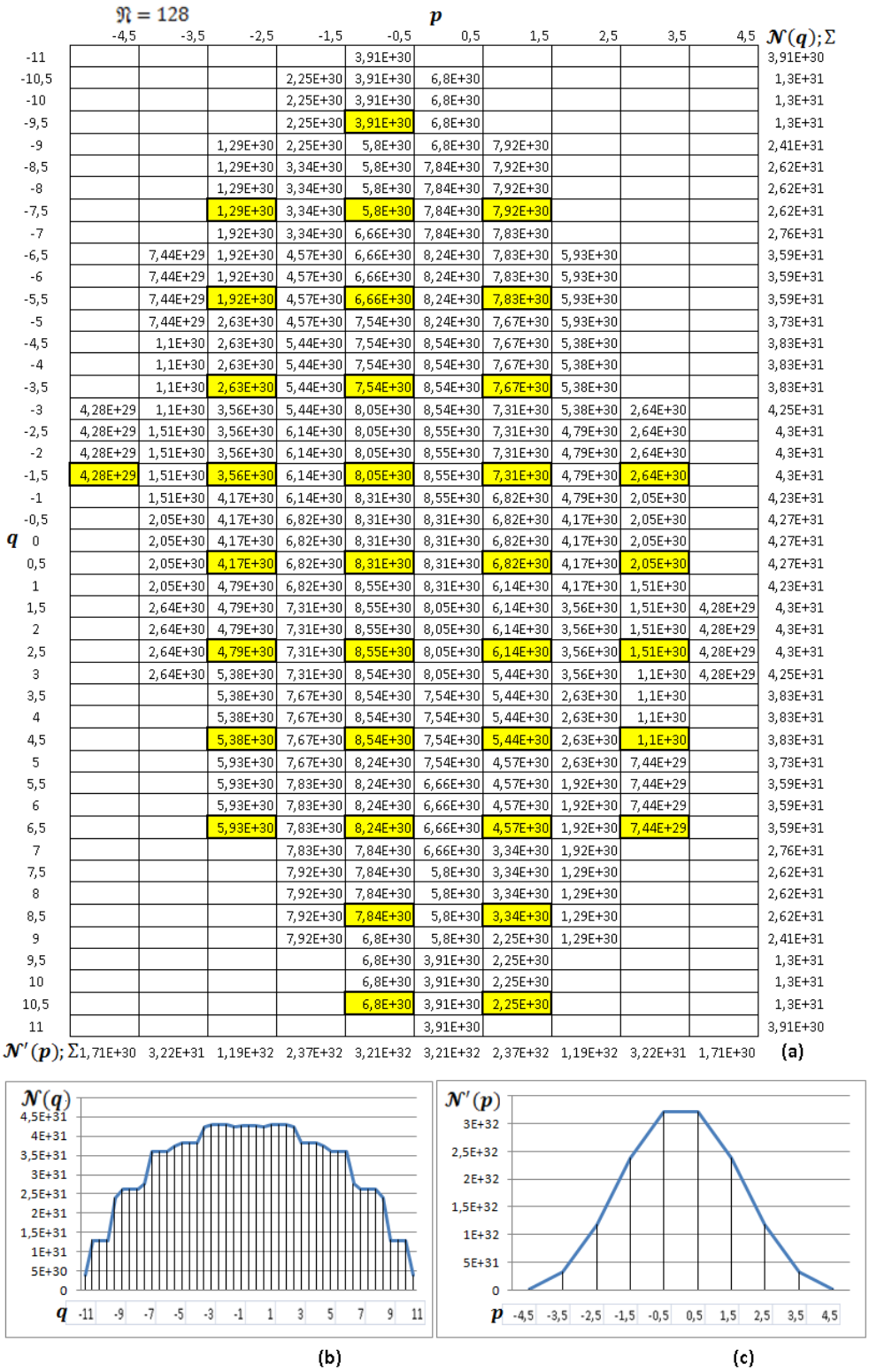

Fig. 11: Results of numerical calculations for the 128th pass of rays, i.e., $\Re = 128$, for eight periodic trajectories of the $[p = (i + 1/2)\gamma,\ q = jk/2]$ system. Thirty five cells (corresponding to 35 rays within one pass in Fig. 10) of one of the eight groups of the system (***K″*** group) are highlighted with the darker color and heavy external borders of the cells (a). The figure also shows the envelopes of distribution of number $\mathbb{N}$ of rays of $\boldsymbol{\mathcal{N}(q)}$ on the section (b) and $\boldsymbol{\mathcal{N}'(p)}$ at the angle (c). Note, according to our calculations, in this case, there is virtually no change in the form of the envelopes, (b) and (c), approximately after the 70th pass.

$[p = (i + 1/2)\gamma,\ q = jk/2]$ system for all the eight groups for $D = 22k$, $\Gamma = 9\gamma$.

The darker cells with heavy external borders shown in Fig. 11 correspond to one of the eight groups of the system (***K″*** group) shown in Fig. 10.

Forms of the envelopes of distribution of the number of rays for the *half-integer system* are similar to the forms of the envelopes for the *integer system* described in [3]. The form of the envelope $\mathcal{N}(q)$ in Fig. 11(b) on the section after a large number of passes (Fig. 11b) is close to a parabola of the fourth degree, and the form of the envelope $\mathcal{N}'(p)$ at the angle (Fig. 11c) is close to Gaussian distribution.

In [3] we noted that the form of the envelope $\mathcal{N}(q)$ on the section for periodic trajectories corresponds to the form of the envelopes of speed distribution at zero pass ($\mathfrak{N} = 0$) and volume distribution after a large number of passes ($\mathfrak{N} \to \infty$) of liquid in pipe section at laminar flow.

In Fig. 11(b) we can see that the envelope $\mathcal{N}(q)$ has a stepped structure compared to the more smooth form of the envelope $\mathcal{N}'(p)$ (Fig. 11c). Similar results were received from numerical calculations for the integer system in [3], but the half-integer model gives the more accurate image of the "steps" compared to the integer model.

It can be assumed that such a stepped structure of the envelope $\mathcal{N}(q)$ explains the existence of layers of final thickness in liquid at laminar flow [8]. The speed and volume of liquid do not change within each of these layers of a certain final thickness.

2 Gaussian (paraxial) rays and Pauli Principle

2.1 Angles, distances and quantum system

Pauli Principle [6, 7] is correct for electrons and other particles with half-integer spin in a quantum system.

The condition of each electron in an atom is characterized by four quantum numbers [6, 7]:

$$\left.\begin{array}{rll} \text{Principal} & n & (n = 1, 2, 3, \dots) \\ \text{Azimuthal} & l & (l = 0, 1, 2, \dots, n-1) \\ \text{Magnetic} & m_l & (m_l = -l, \dots, -1, 0, +1, \dots, +l) \\ \text{Spin} & m_s & \left(m_s = +\tfrac{1}{2},\ -\tfrac{1}{2}\right) \end{array}\right\}. \quad (13)$$

Fig. 23 of the Appendix illustrates an example from [6] of spatial quantization.

In monographs [6] and [7] the spin is also denoted by one letter "s":

$$m_s = s = \pm\frac{1}{2}. \quad (13a)$$

According to Pauli Principle in a quantum system, for example in an atom, there can't be two electrons possessing identical quantum numbers: n, l, m_l, m_s. That is, two electrons cannot be in the same state simultaneously. No more than $2n^2$ electrons can be in a state with n value in an atom [6, 7]. If

$$\left.\begin{array}{ll} n = 1 & \text{there can be 2 electrons} \\ n = 2 & \text{there can be 8 electrons} \\ n = 3 & \text{there can be 18 electrons} \\ \dots\dots\dots\dots\dots\dots\dots\dots & \end{array}\right\}. \quad (14)$$

Electrons having identical value of the quantum number n form a *shell*. Shells consist of *subshells*, differing in value of the quantum number l.

Shells are denoted by characters according to value of n [6] and [7]:

$$\left.\begin{array}{rl} \text{Value of } n & 1\ 2\ 3\ 4\ 5\ 6\ 7\dots \\ \text{Designation of the shell} & K\ L\ M\ N\ O\ P\ Q\dots \end{array}\right\}. \quad (15)$$

The electron which is in condition of $l = 0$ is called an s electron, $l = 1$ — p electron, $l = 2$ — d electron, $l = 3$ — f electron, followed by g, h, etc. alphabetically. The value of the principal quantum number n is specified before the symbol of the azimuthal quantum number l [7].

The division of possible conditions of an electron in an atom into shells and subshells [7] is presented in the form of a *periodic table of conditions* of an electron (see Fig. 24 of the Appendix).

The process of building electron shells [7] (according to Pauli Principle) of the first 36 elements of the Mendeleev Periodic System is presented in the form of a *periodic table of elements* (see Fig. 25 of the Appendix).

Now let's give an algorithm of creation of another specific case of the binary $[p = (i + 1/2)\gamma,\ q = jk/2]$ system of rays of periodic trajectories (considered in Section 1.4). We will begin with the minimum quantity of rays consistently passing to the more complicated configurations of the system. Thus, we will compare the properties of our system to the data provided in periodic tables in Figs. 24 and 25 of the Appendix.

We accept that, for our paraxial beams, all the angles of γn, are small and multiple to the small angle of γ, and the small distance of k is as follows:

$$k \approx \gamma L. \quad (16)$$

For perfect correspondence between our geometric constructions and expressions (13 and 13a), including the data provided in periodic tables in Figs. 24 and 25 of the Appendix, we will enter the following assumptions:

$$\text{Principal number} \quad n \sim \gamma i \sim kj, \quad (n = 1, 2, \dots;\ i = 1, 2, \dots;\ j = 1, 2, \dots), \quad (17)$$

$$\text{Azimuthal number} \quad l = n - 1 \sim \gamma(n-1), \quad (18)$$

$$\text{Magnetic number} \quad m_l = \pm l \sim \pm k(n-1), \quad (19)$$

$$\text{Spin number} \quad s = \pm\frac{1}{2} \sim \pm\frac{\gamma}{2} \text{ and } m_s = \pm\frac{1}{2} \sim \pm\frac{k}{2}. \quad (20)$$

Electron shell	n	l	m_l	m_s	Sub shell
K	1	0	0	↑↓	$K(1s)$

(a)

Element	K	L		M		
	$1s$	$2s$	$2p$	$3s$	$3p$	$3d$
1 H	1	-	-	-	-	-
2 He	2	-	-	-	-	-

(b)

Fig. 12: K shell and the first parts of the periodic tables of (a) conditions of an electron, and (b) elements.

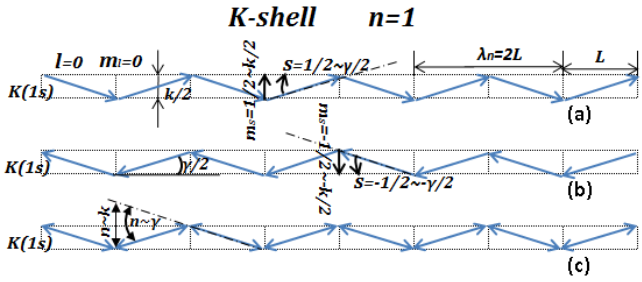

Fig. 13: One of the eight groups of rays of the $\{p=(i+1/2)\gamma\ ,\ q=jk/2\}$ subsystem of periodic trajectories, and K shell. (a) and (b) correspond to an atom of hydrogen, (c) — to an atom of helium. $n=1\sim\gamma\sim k$, $l=0$, $m_l=0$, $s=\pm1/2\sim\pm\gamma/2$, $m_s=\pm1/2\sim\pm k/2$. Dash-dotted lines show axes from which sizes of angles and distances are counted.

Electron shell	n	l	m_l	m_s	Sub shell
L	2	0	0	↑↓	$L_1(2s)$
		1	−1	↑↓	$L_2(2p)$
			0	↑↓	
			+1	↑↓	

(a)

Element	K	L		M		
	$1s$	$2s$	$2p$	$3s$	$3p$	$3d$
3 Li	2	1	-	-	-	-
4 Be	2	2	-	-	-	-
5 B	2	2	1	-	-	-
6 C	2	2	2	-	-	-
7 N	2	2	3	-	-	-
8 O	2	2	4	-	-	-
9 F	2	2	5	-	-	-
10 Ne	2	2	6	-	-	-

(b)

Fig. 14: L shell and the second parts of the periodic tables of (a) conditions of an electron, and (b) elements.

2.2 Periodic tables and geometrical constructions

2.2.1 Creation of the first shell of a quantum system

Fig. 12(a) shows the first (top) part of the periodic table of conditions of an electron (Fig. 24 of the Appendix) describing the first shell of K. Fig. 12(b) shows the top part of the periodic table of elements (Fig. 25 of the Appendix) describing the first two elements:

Fig. 13 shows one of the eight similar to (Figs. 1 and 6) groups of rays of the $[p=(i+1/2)\gamma,\ q=jk/2]$ *system* of periodic trajectories.

These trajectories correspond to the first electron shell of K shown in Fig. 12(a).

To be specific, let's call this *system* of periodic trajectories an $\{p=(i+1/2)\gamma,\ q=jk/2\}$ *subsystem of periodic trajectories* of the $[p=(i+1/2)\gamma,\ q=jk/2]$ *system* of periodic trajectories.

Fig. 13 (a and b) shows two trajectories with opposite (↑ symbol and ↓ symbol) orientation of a spin (one 1s electron). These trajectories correspond to an atom of hydrogen with random orientation of the spin (Fig. 12b).

Fig. 13c shows a trajectory with anti-parallel (↑↓ symbol) spin orientation (two 1s electrons). This trajectory corresponds to an atom of helium (Fig. 12b).

The atom of helium is closing filling of the K shell.

2.2.2 Creation of the second shell of a quantum system

Fig. 14 (a) shows the second part of the periodic table of conditions of an electron (Fig. 24 of the Appendix) describing the second cover of L. Fig. 14 (b) shows the second part of the periodic table of elements (Fig. 25 of the Appendix) describing the elements number three to ten.

Fig. 15 shows one of the eight similar to (Figs. 1 and 6) groups of rays of the $\{p=(i+1/2)\gamma,\ q=jk/2\}$ subsystem of periodic trajectories. These trajectories correspond to the second electron shell of L in Fig. 14 (a and b).

Fig. 15 (a) shows the L shell in the form of a periodic trajectory consisting of the subshell L_1 (one 1s electron) for Li. The form of this shell is the same as in Fig. 13(a) or in Fig. 13(b). The form of K shell for Li is the same as in Fig. 13(c).

Fig. 15 (b, c, d, e, f, g, and h) shows the L shells ($L_1(2s)$ and $L_2(2p)$ subshells) for Be, B, C, N, O, F, and Ne respectively (Fig. 14a and b):

The K shell for these elements is the same as that for Li (see Fig. 13c).

The K shell and L shell of the elements (Figs. 12 to 15) can settle down in our geometric model similar to arrangement of $\boldsymbol{K''}$ group of rays and $\boldsymbol{L''}$ group of rays respectively (Figs. 1, 7 and 8).

The atom of Ne is closing filling the L shell.

2.2.3 Creation of the third and fourth shells of a quantum system

Geometric schemes of Pauli Principle and elements of periodic table are further constructed in compliance with the above algorithm. Therefore, we will confine ourselves to giving specific examples.

The second part of the periodic table of conditions of an electron (Fig. 24 of the Appendix) describing the third M

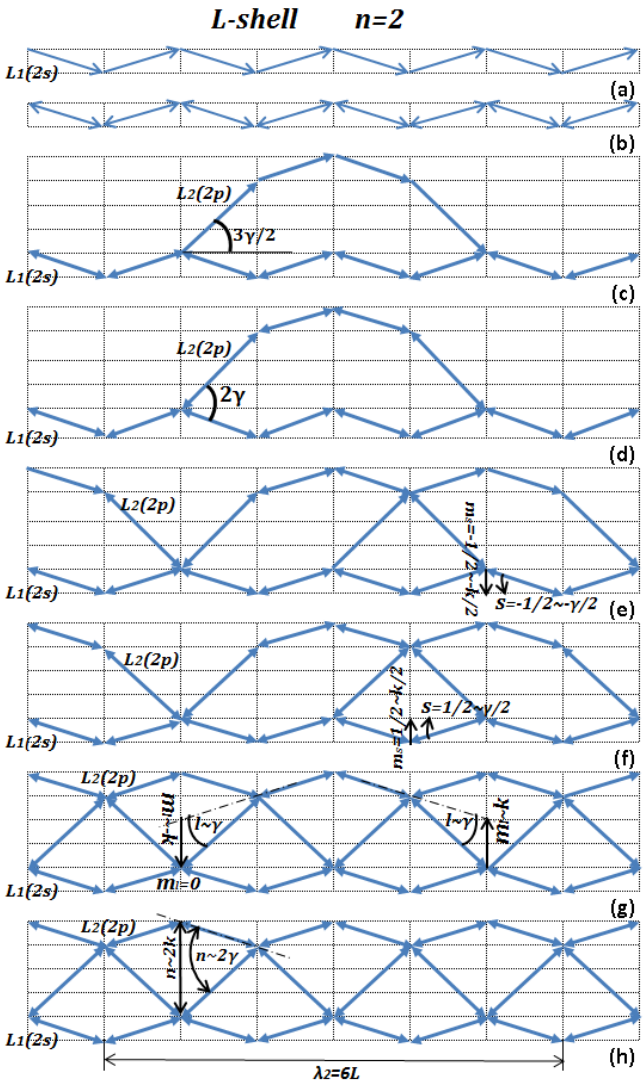

Fig. 15: One of the eight groups of rays of the $\{p=(i+1/2)\gamma,\ q=jk/2\}$ subsystem of periodic trajectories and consecutive process of filling L shell according to Fig. 14 (a and b). Designations of quantum numbers are similar to these in Fig. 13. Dash-dotted lines show axes from which sizes of angles and distances are counted.

shell and the fourth N shell is given in Fig. 16(a). Eight elements of the third part of the periodic table of elements (see Fig. 25 of the Appendix) are given in Fig. 14(b) on a selective basis (see Fig. 16).

Shells of K and L (Fig. 16a) for all the elements shown in Fig. 16(b) are the same as in Fig. 13(c) and Fig. 15(h).

The shell of M ($3s$ subshell) for Na is the same as in Fig. 13(a) or Fig. 13(b).

The subshells $3s$ and $3p$ of the shell of M for Ar and K (Fig. 16b) has the same forms as shown in Fig. 15(h).

The shell of N ($4s$ subshell) for K and Cr (Fig. 16b) is the same as in Fig. 13(a), Fig. 13(b), and Fig. 15(a).

The shell of N ($4s$ subshell) for Sc and Ni is the same as

Electron shell	n	l	m_l	m_s	Sub shell
M	3	0	0	↑↓	$M_1(3s)$
		1	−1	↑↓	$M_2(3p)$
			0	↑↓	
			+1	↑↓	
		2	−2	↑↓	$M_3(3d)$
			−1	↑↓	
			0	↑↓	
			+1	↑↓	
			+2	↑↓	
N	4	0	0	↑↓	$N_1(4s)$
		1	−1	↑↓	$N_2(4p)$
			0	↑↓	
			+1	↑↓	
		2	−2	↑↓	$N_3(4d)$
			−1	↑↓	
			0	↑↓	
			+1	↑↓	
			+2	↑↓	
		3	−3	↑↓	$N_4(4f)$
			−2	↑↓	
			−1	↑↓	
			0	↑↓	
			+1	↑↓	
			+2	↑↓	
			+3	↑↓	

(a)

Element	K	L		M			N	
	$1s$	$2s$	$2p$	$3s$	$3p$	$3d$	$4s$	$4p$
11 Na	2	2	6	1	-	-	-	-
18 Ar	2	2	6	2	6	-	-	-
19 K	2	2	6	2	6	-	1	-
21 Sc	2	2	6	2	6	1	2	-
24 Cr	2	2	6	2	6	5	1	-
28 Ni	2	2	6	2	6	8	2	-
31 Ga	2	2	6	2	6	10	2	1
36 Kr	2	2	6	2	6	10	2	6

(b)

Fig. 16: Shells of M and N, and the third parts of the periodic tables of (a) conditions of an electron, and (b) eight elements.

in Fig. 13(c) and Fig. 15(b).

The shell of N (subshells $4s$ and $4p$) for Ga is the same as in Fig. 15(c).

The shell of N (subshells $4s$ and $4p$) for Kr is the same as in Fig. 15(h).

Fig. 17 (a, b, c, and d) shows the shell of M (subshells 3s, 3p, and 3d) for (Sc), (Cr), (Ni), (Ga and Kr) respectively (Fig. 16a and b):

Three or four shells of K, L, M, and N (Figs. 13 to 17) for the elements can settle down in our geometric model similar to the arrangement of groups of rays of $\boldsymbol{K''}$, $\boldsymbol{L''}$, $\boldsymbol{M''}$, and $\boldsymbol{N''}$ in Figs. 1, 7 and 8.

The geometric schemes of Pauli Principle and elements of the periodic table are also further created in compliance with the above algorithm.

However, our geometric model similar to (Figs. 1 and 6) of groups of rays of the $\{p=(i+1/2)\gamma,\ q=jk/2\}$ subsystem of periodic trajectories consists only of eight groups of rays. Therefore, while remaining within the offered model, it is possible to assume that the number of shells of an atom is no more than eight either. If we continue increasing the number of ray groups to more than eight, the rays will overlap, and the shells will merge.

Thus, if the number of shells does not exceed eight, the total number of elements of the periodic system (14) cannot exceed 128.

Deviations from the sequence of filling the periodic system (e.g., for the elements such as K, etc.) (Fig. 16b) hypothetically reduce (or increase) the total number of elements of the periodic system.

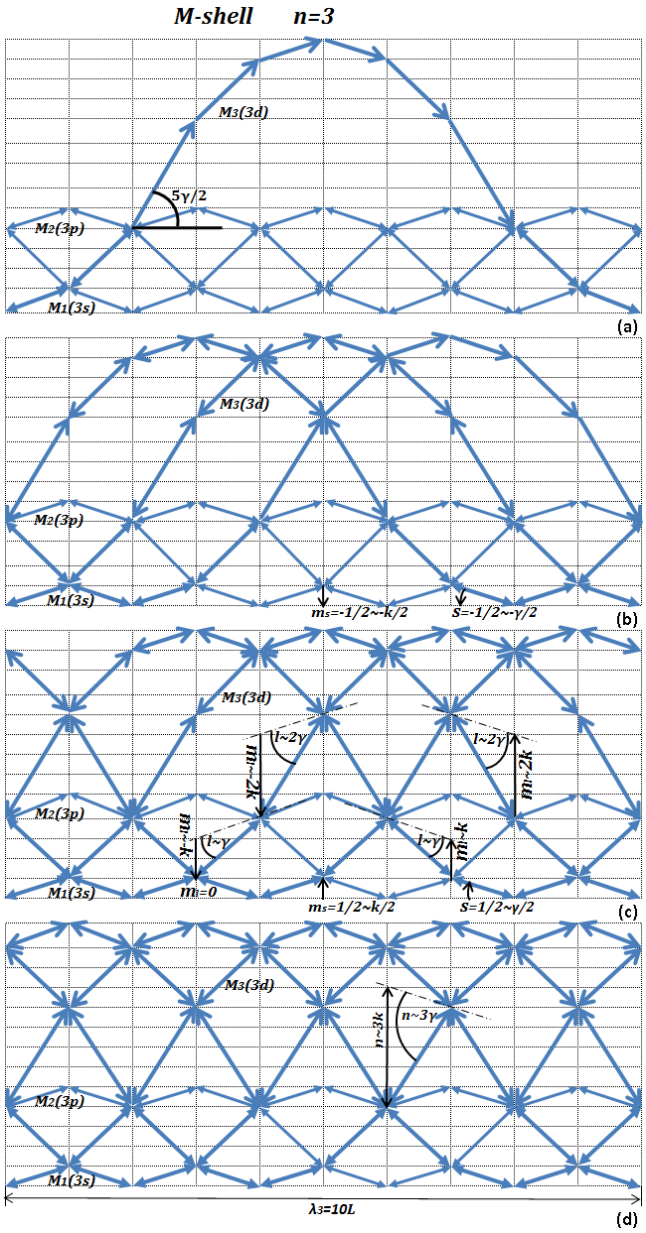

Fig. 17: One of the eight groups of rays of $\{p = (i + 1/2)\gamma,\ q = jk/2\}$ subsystem of periodic trajectories and consecutive process of filling M and N shells for eight elements according to Fig. 16 (a and b). Designations of quantum numbers are similar to these in Figs. 13 and 15. Dash-dotted lines show axes from which sizes of angles and distances are counted.

2.2.4 Pauli Principle and the geometric system of the hydrogen atom

Monographs on quantum mechanics [6] and [7] consider the simplest quantum mechanical system of an atom of hydrogen (Figs. 26 to 28 of the Appendix). Let's make a review of this example too.

Fig. 18 shows the fifth shell of O:

Electron shell	n	ℓ	m_ℓ	m_s	Sub shell
O	5	0	0	⇅	$O_1(5s)$
		1	−1	⇅	$O_2(5p)$
			0	⇅	
			+1	⇅	
		2	−2	⇅	$O_3(5d)$
			−1	⇅	
			0	⇅	
			+1	⇅	
			+2	⇅	
		3	−3	⇅	$O_4(5f)$
			−2	⇅	
			−1	⇅	
			0	⇅	
			+1	⇅	
			+2	⇅	
			+3	⇅	
		5	−4	⇅	$O_5(6g)$
			−3	⇅	
			−2	⇅	
			−1	⇅	
			0	⇅	
			−1	⇅	
			−2	⇅	
			−3	⇅	
			−4	⇅	

Fig. 18: Shell of O of the periodic table of conditions of an electron.

Fig. 19 shows one of the eight groups similar to (Figs. 1 and 6) of rays of the $\{p = (i + 1/2)\gamma,\ q = jk/2\}$ subsystem of periodic trajectories. These trajectories correspond to the fifth electron shell of O shown in Fig. 18. In this example, the O shell is filled completely and contains five subshells.

The $\{p = (i + 1/2)\gamma,\ q = jk/2\}$ subsystem for an atom of hydrogen can be constructed geometrically in accordance with Pauli Principle and similar to the construction method described in previous Sections.

The $\{p = (i + 1/2)\gamma,\ q = jk/2\}$ subsystem shown in Fig. 19 is in many respects similar to the $[p = (i + 1/2)\gamma,\ q = jk/2]$ system in Fig. 10, but contains the smaller quantity of rays and the smaller quantity of the wavy trajectories consisting of these rays.

The wavy trajectories shown in Fig. 19 settle down in the lower part of the coordinate grid and are "attached" to the lower horizontal unlike the wavy trajectories in Fig. 10, which can settle down in any part of the coordinate grid within D size.

In principle, the creation of the O shell in Fig. 19 does not differ from creation of other shells shown in Figs. 13, 15, 17.

Upon comparison of angles multiple p in Fig. 10 and multiple n in Fig. 19, it can be seen that the relationship between these angles is as follows:

$$n \sim |p| + \frac{1}{2}\,. \tag{21}$$

In Fig. 19 we illustrated the allowed quantum transitions [6] and [7]:

$$\Delta n = \pm 1 \quad \text{and} \quad \Delta l = \pm 1 \tag{22}$$

in the form of angles, but not distances as in Figs. 26 to 28 of the Appendix. However, considering ratios (16 to 20) for small angles, sizes (22) can be illustrated (in principle) in the form of distances as well, since:

$$\Delta n = \pm 1 \sim \pm\gamma \sim \pm k \quad \text{and} \quad \Delta l = \pm 1 \sim \pm\gamma \sim \pm k\,. \tag{23}$$

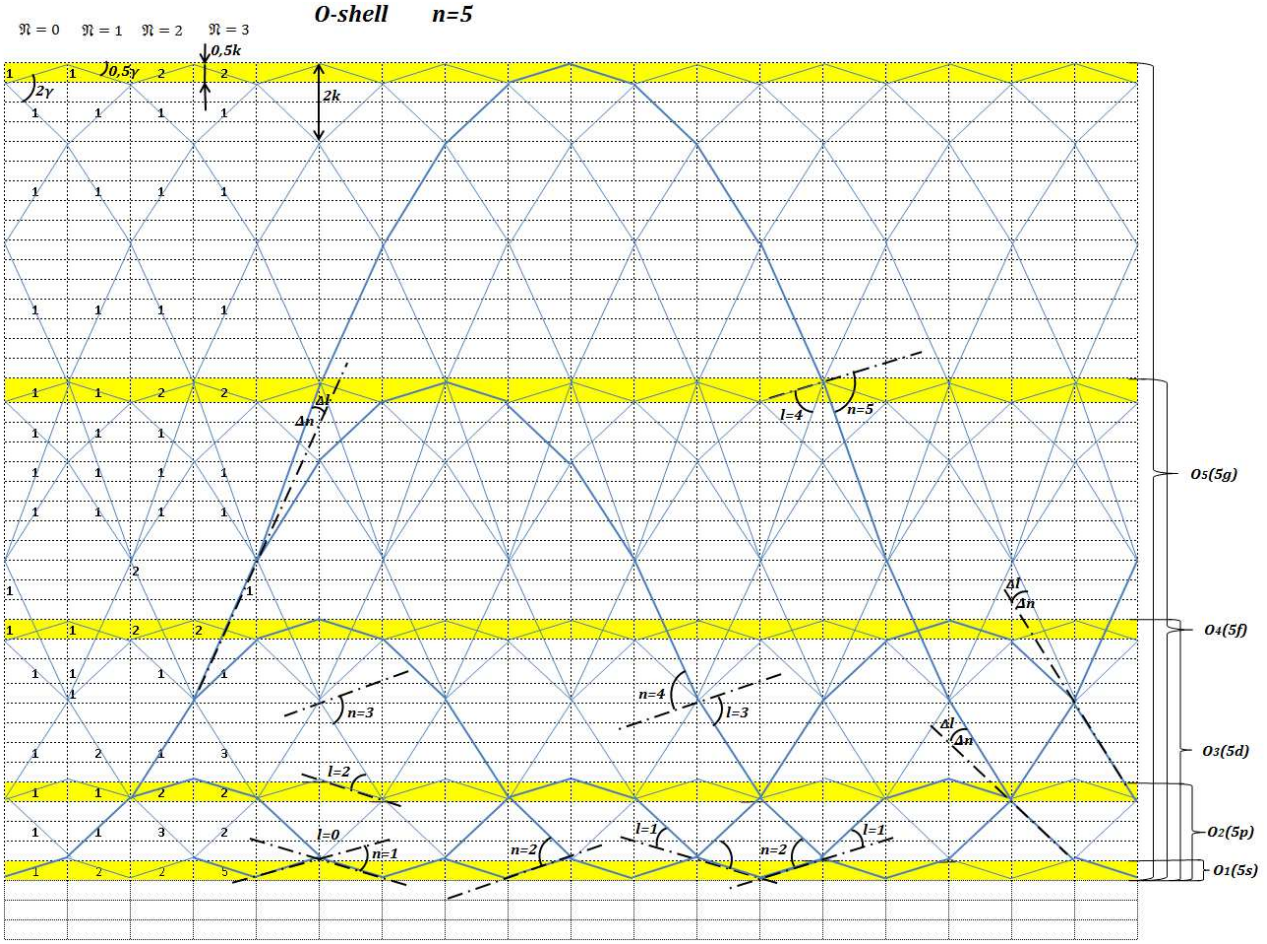

Fig. 19: One of the eight groups of rays of the considered $\{p = (i + 1/2)\gamma,\ q = jk/2\}$ subsystem of periodic (wavy) trajectories. The shell of O is completely filled according to Fig. 18. This group contains 15 links ($\mathbb{K} = 15$) within one pass of $\mathfrak{R}$. Troughs of the "waves" are located ("attached to") only on the lower horizontal, while crests of the "waves" are located ("attached to") on several higher horizontals. The horizontals are marked in separate color. These horizontals have thickness of $0,5k$ and are located at the increasing distance of $2kn$ from each other from the bottom upwards. The designations of the quantum numbers are similar to these in Figs. 13 to 17. Dash-dotted lines show axes from which sizes of angles and distances are counted. Quantum transitions $\Delta n = \pm 1$ and $\Delta l = \pm 1$ are shown in the form of angles between dash-dotted lines. On the right, location of five subshells is indicated by curly braces. Figures put next to links (for $\mathfrak{R} = 0 - 3$) show the number of rays of $\mathbb{N}$ and the process of summation of rays spreading along the links.

Fig. 20 gives images of layers of a nonlinear arithmetic parallelepiped and a numerical example of calculation of O shell of the $\{p = (i + 1/2)\gamma,\ q = jk/2\}$ subsystem of periodic trajectories (Fig. 19) for zero and the subsequent three passes of rays, i.e. for $\mathfrak{R} = 0 - 4$. Four rectangles shown in Fig. 20 are the layers of the nonlinear arithmetic parallelepiped.

n and l values are given on the right in Fig. 20 with taking into account the ratios (18 and 21).

The calculation was made according to the rule (3) of consecutive filling of an arithmetic rectangle with numbers taking into account the *first* and the *second* threshold (4 and 5; 8 and 9) and initial (6, 7, and 10) conditions, including the algorithm (8 to 10).

Each of the four layers of the arithmetic parallelepiped shown in Fig. 20 is similar to the layer represented in Fig. 11, but there are differences as well. Therefore, it is necessary to set the *third* threshold conditions. We took these conditions for our example directly from Fig. 19. As this approach is illustrative for us, the total number of rays is not that big. All the wavy trajectories are "attached" to the lower horizontal. The *third* threshold conditions can be set in other illustrative ways, e.g., by means of special nomograms.

Thus, we made calculations in Excel according to expression (3). The appropriate formulas for the respective p and q can be taken from Fig. 3 or Fig. 7, for example.

Fig. 21 shows results of numerical calculations of layers of the nonlinear arithmetic parallelepiped for O shell (Fig. 20) in Excel are given in the form of envelopes of distribution of the ray number. In a, c, e, g, and i (the left column), you can see the envelopes of distribution of the ray number at the an-

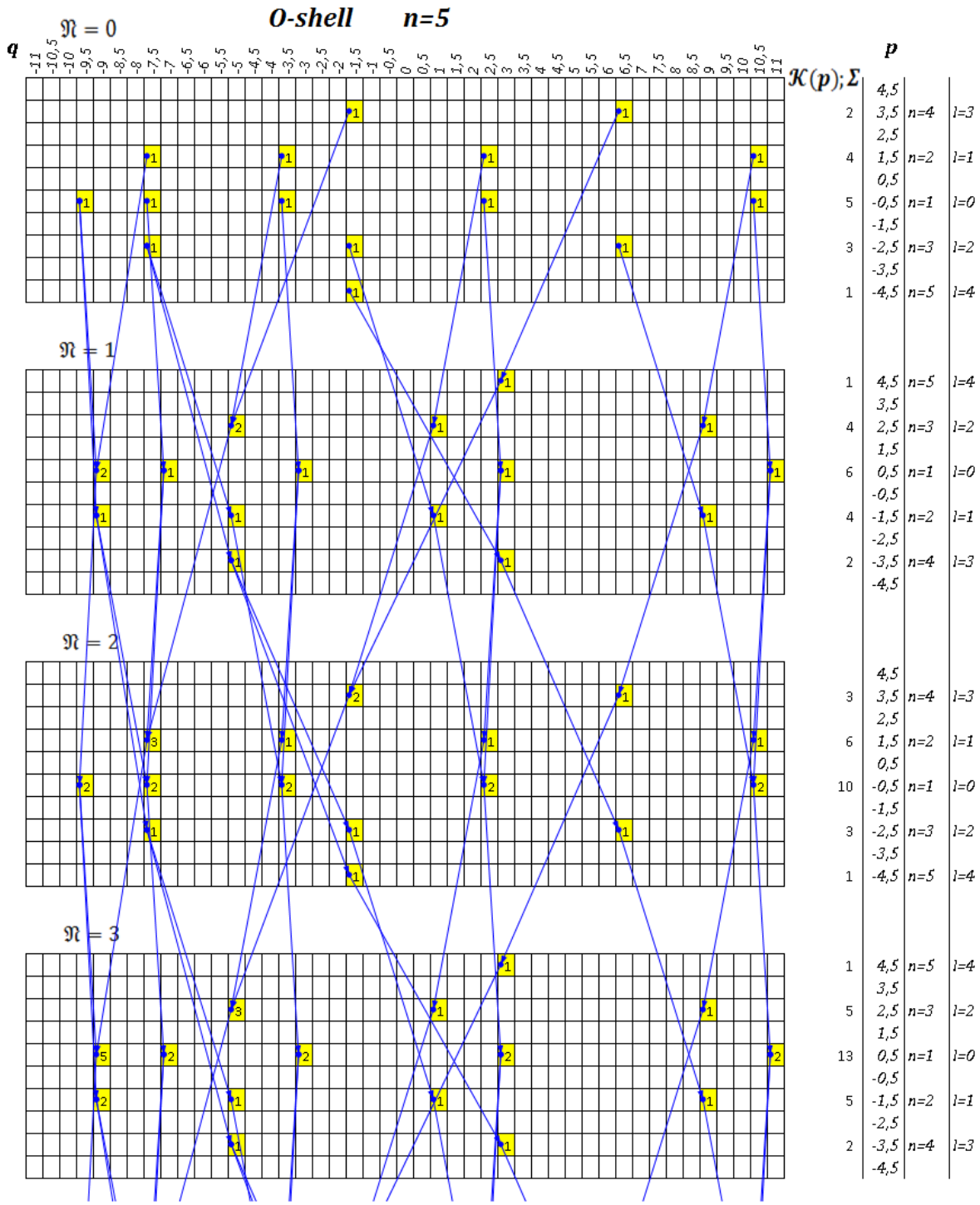

Fig. 20: One of the eight groups of rays of the $\{p=(i+1/2)\gamma,\ q=jk/2\}$ subsystem of periodic (wavy) trajectories. The O shell is completely filled according to Figs. 18 and 19. Numerical calculation in Excel was made for the first four passes of rays (iterations). Arrows show dependent cells. Fifteen highlighted cells within one pass of $\mathfrak{N}$ (one layer of a parallelepiped) correspond to fifteen links ($\mathbb{K}=15$) within one pass of $\mathfrak{N}$ shown in Fig. 19. Figures in the highlighted cells correspond to the number of rays of $\mathbb{N}$ extending along the links of $\mathbb{K}$.

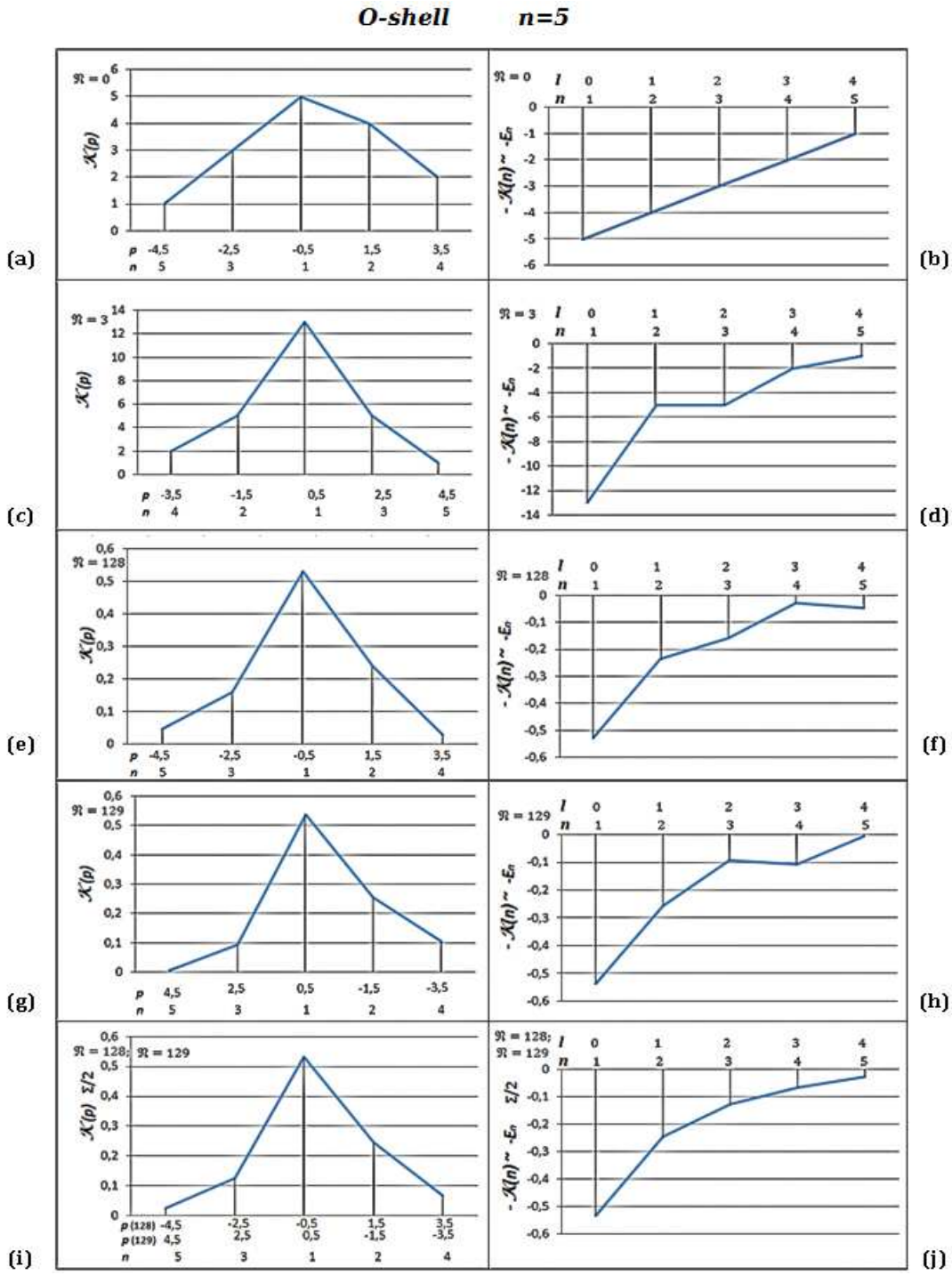

Fig. 21: This Figure shows the results of numerical calculations (Fig. 20) for $\mathfrak{N} = 0$, 32, 128, 129 (a to h) of the completely filled O shell for the $\{p = (i + 1/2)\gamma,\ q = jk/2\}$ subsystem of periodic (wavy) trajectories. The envelopes of distribution of the ray number at the angle $\mathcal{K}(p)$ are given in the left column. The envelopes of distribution of the ray number at the angle $\mathcal{K}(n)$ are given in the right column. The shared envelopes for $\mathfrak{N} = 128, 129$ are given in (i and j). Graphs (e to j) are shown in a normalized form. Note, according to our calculations, in this case, there is virtually no change in the form of the envelope approximately after the 70th pass.

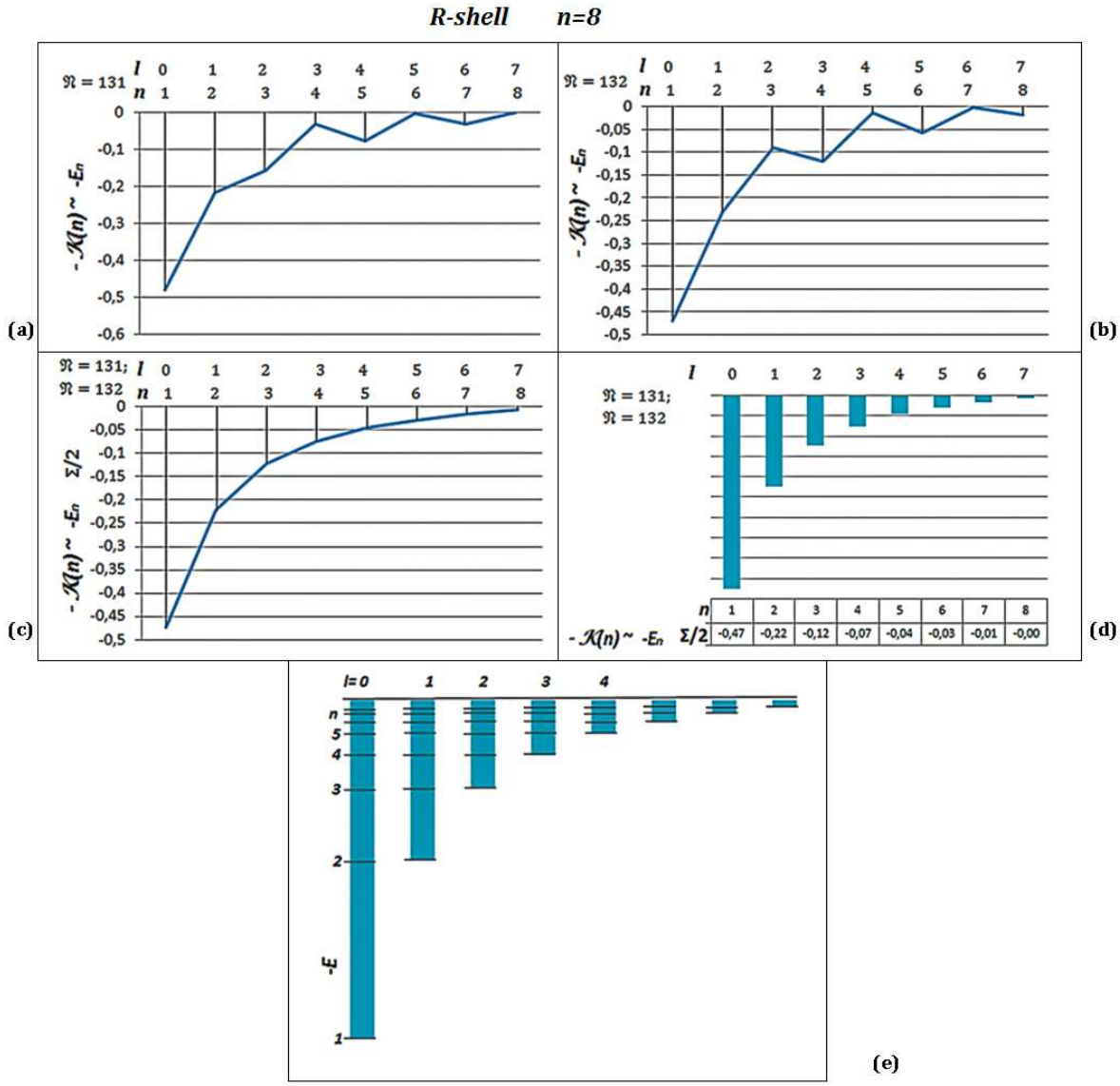

Fig. 22: This Figure shows results of numerical calculations of the completely filled 8th shell of R for the $\{p=(i+1/2)\gamma,\ q=jk/2\}$ subsystem of periodic (wavy) trajectories. In (a) and (b), you can see the envelopes of distribution of the ray number at the angle $\mathcal{K}(n)$ for passes $\mathfrak{R}=131,132$. Results of joint calculations for passes $\mathfrak{R}=131$ and $\mathfrak{R}=132$ in the form of the envelope are given in (c) and these in a form of histograms are given in (d) and (e). Envelopes (a to c) and histograms (d and e) are presented in the normalized form. Note, according to our calculations, in this case, there is virtually no change in the form of envelopes approximately after the 100th pass ($\mathfrak{R}=100$). The histogram in (e) is similar to Fig. 28 of the Appendix.

gle $\mathcal{K}(p)$. In b, d, f, h, and j (the right column), you can see the envelopes of distribution of the ray number at the angle $\mathcal{K}(n)$ (taking into account expression (21). The results of numerical calculation for zero pass of rays, i.e. for $\mathfrak{R}=0$, are given in a and b; for $\mathfrak{R}=3$ — in c and d; for $\mathfrak{R}=128$ — in e and f; and for $\mathfrak{R}=129$ — in g and h.

Shared graphs of $\mathcal{K}(p)$ and $\mathcal{K}(n)$ for $\mathfrak{R}=128$ and $\mathfrak{R}=129$ are given in i and j, namely:

$$\mathcal{K}(p)_{\mathfrak{R}=128,\ \mathfrak{R}=129}=\frac{1}{2}\left[\mathcal{K}(p)_{\mathfrak{R}=128}+\mathcal{K}(p)_{\mathfrak{R}=129}\right] \quad (24)$$

and

$$\mathcal{K}(n)_{\mathfrak{R}=128,\ \mathfrak{R}=129}=\frac{1}{2}\left[\mathcal{K}(n)_{\mathfrak{R}=128}+\mathcal{K}(n)_{\mathfrak{R}=129}\right], \quad (25)$$

where $\mathcal{K}(p)$ and $\mathcal{K}(n)$ are in the normalized form.

In this work, like in previous works [2] to [5], we assume that the number of rays of $\mathbb{N}$ extending along the number of multiplicative links of $\mathbb{K}$ is proportionate to energy. For negative energy of an electron — E extending along these rays,

we have the following:

$$|E_n| \sim \mathcal{K}(n), \tag{26}$$

$$|E_n| \sim \mathcal{K}(n)_{\mathfrak{R},\,\mathfrak{R}+1}. \tag{27}$$

If we consider Fig. 21 (f and h) and especially Fig. 21(j), we will see that the form of the envelope after a large number of passes resembles more of a hyperbole of the following type:

$$E_n \sim -1/n^2. \tag{28}$$

This ratio obtained from our geometric constructions corresponds to experimental results in spectroscopy and theoretical results of Bohr's theory and quantum mechanics [6] and [7].

Fig. 22 shows the results (similar to those that were shown in Fig. 21 f, h, and j) of numerical calculations of layers of the nonlinear arithmetic parallelepiped for the eighth R shell in the form of envelopes of distribution of the ray number. In (a) and (b), you can see the envelopes of distribution of the ray number at the angle $\mathcal{K}(n)$ for passes of rays $\mathfrak{R} = 131$, 132. Results of joint calculations for passes of $\mathfrak{R} = 131$ and $\mathfrak{R} = 132$ in the form of the envelope are given in (c), and these in a form of histograms are given in (d) and (e).

If we consider Fig. 22 (a and b) and especially Fig. 22 (c to e), we will see that the form of the envelope after a large number of passes resembles more of a hyperbole (28).

Fig. 22 (e) similar to Fig. 22 (c and d) should be compared to Fig. 28 of the Appendix.

Our numerical calculations show that with an increase in the number of passes of $\mathfrak{R}$, and an increase in the number of subshells of a shell and the main number n, the form of an envelope, Fig. 21 (j) and Fig. 22 (c), increasingly resembles a hyperbole of (28) type. If the number of subshells exceeds eight (e.g., you can construct eleven), eight of eleven subshells can be subsumed to subshells, while the rest three can be subsumed to a continuous spectrum [6] and [7]. Such creation of a continuous spectrum does not contradict Pauli Principle.

Conclusions

In our illustrative geometric researches, using just one basic summation formula of $A = B + C$ (3), Excel, and various initial and threshold conditions set, we have revealed a number of new regularities like we did in previous works [3] and [4].

It appeared that quantum systems can be geometrically interpreted by means of our model of a half-integer rays system in an illustrative way.

We have described Pauli Principle, shells and subshells of atoms of the periodic table. At the same time, the number of shells and subshells in our model does not exceed eight, and all the subshells starting with the ninth can be considered a continuous spectrum.

By means of our model, it is possible to interpret the principle, azimuthal, magnetic, and spin quantum numbers in the form of angles and distances.

By means of our model, we have given a separate geometric interpretation of an atom of hydrogen and its power levels. We have interpreted transitions of an electron from one level to another in the form of angles, but not distances as it is commonly interpreted [6] and [7]. In this work, we have also shown that the hyperbolic dependence of energy of a hydrogen atom of $E_n \sim -1/n^2$ (28) known from experimental spectral studies, Bohr's theory and quantum mechanics, can be also obtained from our geometric constructions on the basis of Pauli Principle.

Based on the research of a half-integer ray model, we have illustrated the stepped structure of layers at laminar flow of liquid [8]. The similar stepped structure was observed in research of integer ray model made by us in [3], but the half-integer model gives the more accurate image of "steps" in comparison with our integer model.

Acknowledgements

The author expresses gratitude to the late Prof. E. E. Shnoll, Prof. J. Peters (Canada), Prof. V. V. Dikusar (Russia), Prof. S. E. Shnoll (Russia), Prof. A. A. Rukhadze (Russia), Prof. V. G. Mikhalevich (Russia), Prof. A. V. Kaganov (Russia), Prof. R. Mehta (India), Dr. A. Shemetov (Russia), Dr. O. Nersesyan (Russia) and Captain V. Kabanov (Russia) for useful discussion and support. The author is also grateful to the Prof. N. J. A. Sloane (USA) for his surprising tables and to the Excel software creators for their excellent Excel.

Submitted on December 26, 2015 / Accepted on January 19, 2015

References

1. Peters J. F., Tozzi A. The Borsuk-Ulam theorem explanes quantum entangement. *Technical Reports*, November 2015, DOI: 10.13140/RG.2.1.3860.1685.
2. Yurkin A. V. Quasi-resonator a new interpretation of scattering in lasers. *Quantum Electronics*, 1994, v. 24, 359.
3. Yurkin A. V. Symmetric Triangle of Pascal and Arithmetic Parallelepiped. On Possibility of New Evident Geometrical Interpretation of Processes in Long Pipes. Lambert Academic Publishing, 2015.
4. Yurkin A. V. New Binomial and New View on Light Theory. About One New Universal Descriptive Geometric Model. Lambert Academic Publishing, 2013.
5. Yurkin A. V. Recurrence calculation of laser divergence and refractive analog of a multilobe mirror. *Quantum Electronics*, 1993, v. 23, 323.
6. Putilov K. A., Fabrikant V. A. The Course of Physics. Vol. 3. Moscow, Fizmatgiz, 1960 (in Russian).
7. Savelyev I. V. The General Course of Physics. Vol. 3. Moscow, Nauka, 1982 (in Russian).
8. Putilov K. A. The Course of Physics. Vol. 1. Moscow, Fizmatgiz, 1954 (in Russian).

Appendix: reference tables

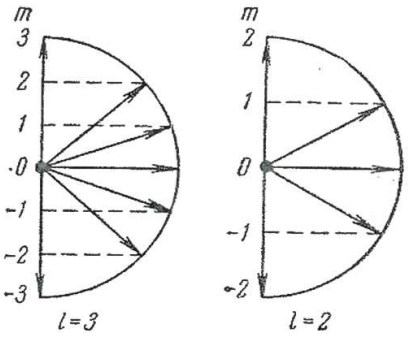

Fig. 23: Illustration of the principle of spatial quantization. Possible values of projections of the orbital momentum to the direction of a magnetic field for $l = 3$ and $l = 2$. (Fig. 231 from [6]).

Shell	n	l	m_l	m_s	Subshell	Shell	n	l	m_l	m_s	Subshell
K	1	0	0	↑↓	$K(1s)$	N	4	0	0	↑↓	$N_1(4s)$
L	2	0	0	↑↓	$L_1(2s)$			1	−1	↑↓	$N_2(4p)$
		1	−1	↑↓	$L_2(2p)$				0	↑↓	
			0	↑↓					+1	↑↓	
			+1	↑↓				2	−2	↑↓	$N_3(4d)$
M	3	0	0	↑↓	$M_1(3s)$				−1	↑↓	
		1	−1	↑↓	$M_2(3p)$				0	↑↓	
			0	↑↓					+1	↑↓	
			+1	↑↓					+2	↑↓	
		2	−2	↑↓	$M_3(3d)$			3	−3	↑↓	$N_4(4f)$
			−1	↑↓					−2	↑↓	
			0	↑↓					−1	↑↓	
			+1	↑↓					0	↑↓	
			+2	↑↓					+1	↑↓	
									+2	↑↓	
									+3	↑↓	

Fig. 24: Division of possible conditions of an electron in an atom into shells and subshells. (Table 36.1 from [7]).

Element	K	L		M			N		Basic therm
	1s	2s	2p	3s	3p	3d	4s	4p	
1 H	1	—	—	—	—	—	—	—	$^2S_{1/2}$
2 He	2	—	—	—	—	—	—	—	$^1S_0$
3 Li	2	1	—	—	—	—	—	—	$^2S_{1/2}$
4 Be	2	2	—	—	—	—	—	—	$^1S_0$
5 B	2	2	1	—	—	—	—	—	$^2P_{1/2}$
6 C	2	2	2	—	—	—	—	—	$^3P_0$
7 N	2	2	3	—	—	—	—	—	$^4S_{3/2}$
8 O	2	2	4	—	—	—	—	—	$^3P_2$
9 F	2	2	5	—	—	—	—	—	$^2P_{3/2}$
10 Ne	2	2	6	—	—	—	—	—	$^1S_0$
11 Na	2	8		1	—	—	—	—	$^2S_{1/2}$
12 Mg	2	8		2	—	—	—	—	$^1S_0$
13 Al	2	8		2	1	—	—	—	$^2P_{1/2}$
14 Si	2	8		2	2	—	—	—	$^3P_0$
15 P	2	8		2	3	—	—	—	$^4S_{3/2}$
16 S	2	8		2	4	—	—	—	$^3P_2$
17 Cl	2	8		2	5	—	—	—	$^2P_{3/2}$
18 Ar	2	8		2	6	—	—	—	$^1S_0$
19 K	2	8		8		—	1	—	$^2S_{1/2}$
20 Ca	2	8		8		—	2	—	$^1S_0$
21 Sc	2	8		8		1	2	—	$^2D_{3/2}$
22 Ti	2	8		8		2	2	—	$^3F_2$
23 V	2	8		8		3	2	—	$^4F_{3/2}$
24 Cr	2	8		8		5	1	—	$^7S_3$
25 Mn	2	8		8		5	2	—	$^6S_{5/2}$
26 Fe	2	8		8		6	2	—	$^5D_4$
27 Co	2	8		8		7	2	—	$^4F_{9/2}$
28 Ni	2	8		8		8	2	—	$^3F_4$
29 Cu	2	8		8		10	1	—	$^2S_{1/2}$
30 Zn	2	8		8		10	2	—	$^1S_0$
31 Ga	2	8		8		10	2	1	$^2P_{1/2}$
32 Ge	2	8		8		10	2	2	$^3P_0$
33 As	2	8		8		10	2	3	$^4S_{3/2}$
34 Se	2	8		8		10	2	4	$^3P_2$
35 Br	2	8		8		10	2	5	$^2P_{3/2}$
36 Kr	2	8		8		10	2	6	$^1S_0$

Fig. 25: The process of building electron shells of the first 36 elements of the periodic system. (Table 37.1 from [7]).

Appendix: reference tables (continue)

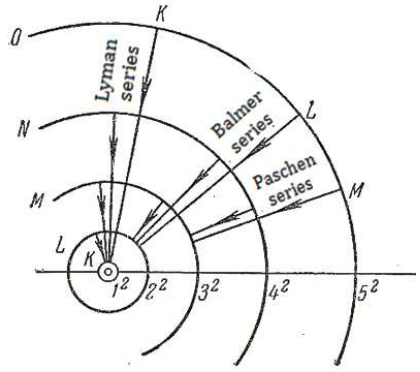

Fig. 26: Orbits of a hydrogen atom in Bohr's theory. The radial arrows located between circles show transitions of an electron from one level to another. (Fig. 228 from [6]).

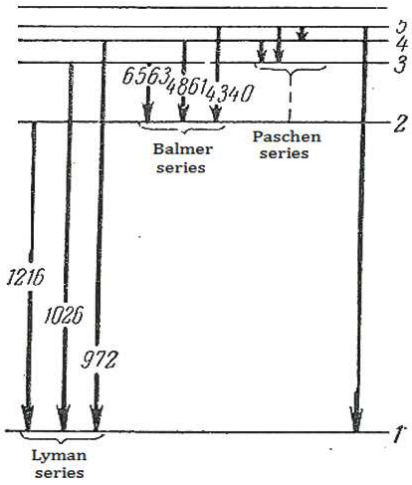

Fig. 27: Scheme of levels of energy of a hydrogen atom. The vertical arrows located between horizontal lines show transitions of an electron from one level to another. (Fig. 229 from [6]).

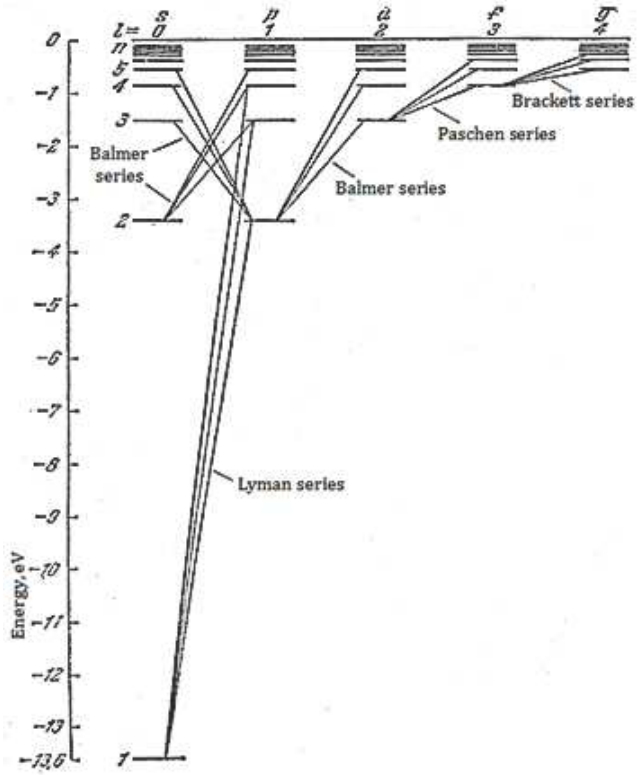

Fig. 28: Scheme of levels of energy of a hydrogen atom. The inclined lines located between horizontal lines show transitions of an electron from one level to another according to the rule of selection $\Delta l = \pm 1$. It means that only transitions upon which l changes by unit are possible. (Fig. 28.1 from [7]).